Realizing Valley-Polarized Energy Spectra in Bilayer Graphene Quantum Dots via Continuously Tunable Berry Phases

Ya-Ning Ren,[1,*] Qiang Cheng,[2,3] Qing-Feng Sun,[3,4,5,*] and Lin He[1,†]

[1]*Center for Advanced Quantum Studies, Department of Physics, Beijing Normal University, Beijing 100875, China*
[2]*School of Science, Qingdao University of Technology, Qingdao, Shandong 266520, China*
[3]*International Center for Quantum Materials, School of Physics, Peking University, Beijing 100871, China*
[4]*Collaborative Innovation Center of Quantum Matter, Beijing 100871, China*
[5]*Beijing Academy of Quantum Information Sciences, West Building #3, No. 10 Xibeiwang East Road, Haidian District, Beijing 100193, China*

(Received 16 August 2021; revised 8 November 2021; accepted 25 April 2022; published 20 May 2022)

The Berry phase plays an important role in determining many physical properties of quantum systems. However, tuning the energy spectrum of a quantum system via Berry phase is comparatively rare because the Berry phase is usually a fixed constant. Here, we report the realization of an unusual valley-polarized energy spectra via continuously tunable Berry phases in Bernal-stacked bilayer graphene quantum dots. In our experiment, the Berry phase of electron orbital states is continuously tuned from about π to 2π by perpendicular magnetic fields. When the Berry phase equals π or 2π, the electron states in the two inequivalent valleys are energetically degenerate. By altering the Berry phase to noninteger multiples of π, large and continuously tunable valley-polarized energy spectra are realized. Our result reveals the Berry phase's essential role in valleytronics and the observed valley splitting, on the order of 10 meV at a magnetic field of 1 T, is about 100 times larger than Zeeman splitting for spin, shedding light on graphene-based valleytronics.

DOI: 10.1103/PhysRevLett.128.206805

In two-dimensional honeycomb lattice systems with broken spatial inversion symmetry, the Berry curvature in two inequivalent valleys has opposite signs, which enables the control of valley degrees of freedom [1–10]. Among various material candidates for valleytronics, gapped Bernal-stacked bilayer graphene (BLG) showing great promise in terms of tunability of the valley current and valley splitting [6–19] is one of the most studied systems. The opposite Berry curvature and the associated magnetization of electron states in the two valleys of the gapped BLG lead to a large linear magnetic field valley splitting, which has been demonstrated recently by single-carrier measurements (in the Coulomb blockade regime) in BLG-based quantum dot (QD) devices [11–15,18]. Besides the Berry-curvature effects, it was also predicted to realize valley-polarized energy spectra in BLG QDs when the Berry phase is tuned to noninteger multiples of π [19]. Yet, in most cases studied to date, the Berry phase in graphene systems equals the integer multiples of π [20–25], and altering the Berry phase to noninteger multiples of π has remained elusive. Therefore, a direct observation of the Berry-phase-induced valley-polarized energy spectrum is still lacking [26].

In this Letter, unusual valley-polarized energy spectra are realized in the BLG QDs via continuously tuning the Berry phase of electron orbital states from about π to 2π. In our experiment, a scanning tunneling microscope (STM) tip is used to approach the BLG to introduce a movable confining potential, i.e., a QD, in the BLG beneath the tip [4,5,13,25,27]. By applying a perpendicular magnetic field, the Berry phase of bound states in the BLG QD is continuously tuned from about π to 2π. When the Berry phase becomes noninteger multiples of π, valley-polarized energy spectra with tunable valley splitting are directly observed.

The Berry phase is the flux of the Berry curvature integrated over the area circled by the closed path in momentum space. In graphene QD, a magnetic field enables fine control of the trajectories and hence the Berry phase for individual confined states [18,25,28], as summarized in Fig. 1 (see Supplemental Material for details [29]). Therefore, graphene QD offers an ideal platform to study the effect of the Berry phase on the energy spectrum. The results obtained in monolayer graphene QD and the BLG QD are quite different. For monolayer graphene, the Berry phase jumps from 0 to π at a critical value of the magnetic field because the Berry curvature is only nonzero at the Dirac point: The Berry phase is zero (π) when their corresponding momentum-space loop does not (does) enclose the Dirac point [Figs. 1(b) and 1(c)]. The π shift of the Berry phase will suddenly lift the degeneracy of the quasibound states with opposite angular momenta $\pm m$ [25,39,40]. For the BLG, the Berry curvature is ring shaped in momentum space [Fig. 1(e)]. Then, the area circled by

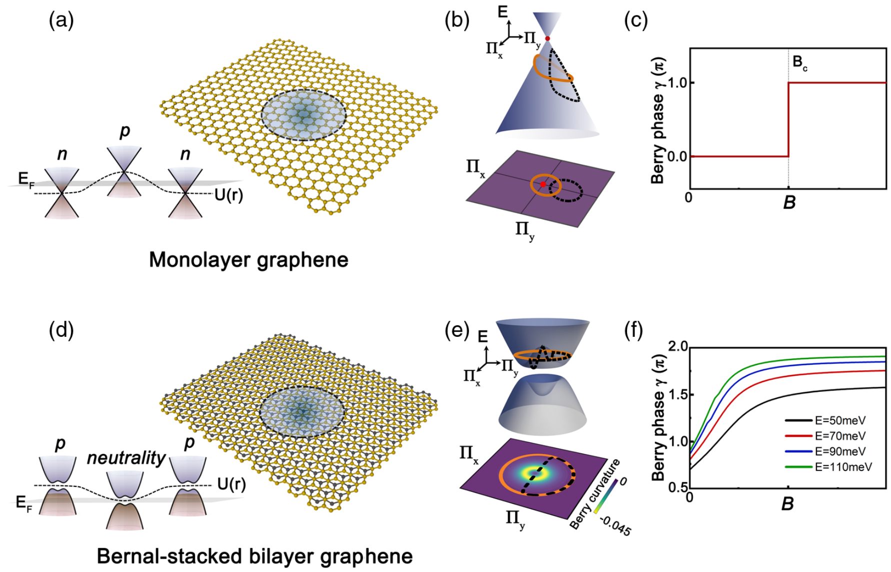

FIG. 1. (a)–(c) Jump of the Berry phase in monolayer graphene QDs. (d)–(f) Continuously tunable Berry phase in Bernal-stacked BLG QDs. (a),(d) Sketches of monolayer graphene QD and BLG QD, respectively. (b),(e) Schematic charge trajectories in momentum space of monolayer graphene QD and BLG QD, respectively. The orange solid and black dashed lines in (b) represent trajectories in the magnetic fields above and below the B_C, respectively. The orange solid and black dashed lines in (e) represent trajectories in the magnetic fields of $10T$ and $0T$, respectively. (c),(f) Berry phase as a function of the magnetic fields B in monolayer graphene QD and BLG QD, respectively.

the closed path and, simultaneously, the Berry phase, can be continuously tuned by the magnetic field [Fig. 1(f)]. When the Berry phase becomes noninteger multiples of π, the energy of the bound states for the two valleys becomes different according to the Einstein-Brillouin-Keller (EBK) quantization rule [19]. Then, an unusual valley-polarized energy spectrum can be obtained.

Our experiments were carried out on decoupled Bernal-stacked BLG on graphite [9,23,41,42] by using a high-magnetic-field STM at $T = 4.2$ K [29]. The decoupled Bernal-stacked BLG is identified by both the STM image and scanning tunneling spectroscopy (STS) spectra (Fig. 2). The atomic-resolution STM image exhibits a triangular lattice [Fig. 2(a)] arising from the A/B atoms' asymmetry in the Bernal-stacked BLG. The high-magnetic-field STS spectra show well-defined Landau quantization of massive Dirac fermions [Figs. 2(b) and 2(c)], which demonstrates explicitly that the studied system is decoupled Bernal-stacked BLG [9,23,41,42] (see Supplemental Material Fig. S1 [29]). In zero magnetic field, the tunneling spectrum exhibits a pronounced peak at the edge of the conduction band [Figs. 2(b), 2(f), and Fig. S2 [29]], indicating emergence of a flat band in the Bernal-stacked BLG. Such a feature was also observed in similar systems in the literature [41,42]; however, it has been ignored in discussions so far. Recently, angle-resolved photoemission measurements for Bernal-stacked BLG on SiC demonstrated the formation of the flat band in the BLG due to the interaction of the substrate [43]. According to our experimental result and calculation, the graphite substrate introduces interlayer asymmetry (hence, the gap in the BLG), leading to the flat band. The band structure is extremely flat, showing a 0.084-meV dispersion, around the conduction band edge [Figs. 2(d)–2(f)]. Therefore, the full width at half maximum of the flat band in the BLG measured in our experiment is comparable to that in magic-angle twisted bilayer graphene (MATBG) (also measured by using STM) [44–49], and it is reasonable to observe correlated phases when it is partially filled [50].

To introduce the BLG QDs in our study, we used a STM tip as a top gate to generate band bending of the BLG beneath the tip [4,5,13,25,27]. In the experiment, the distance between the tip and the sample is shortened by about 0.5 nm (see Fig. S3 in the Supplemental Material for more data [29]) by increasing the tunneling current with a fixed voltage bias, as shown in Fig. 3. For short tip-sample distance, the signal of the flat band is further enhanced in the tunneling spectra [Fig. 3(a); here, $g(V_b, r = 0, B = 0) = dI/dV_b$ reflects the local density of states (LDOS) in the center of the graphene resonator at $B = 0$ T as a function of V_b]. Besides that, the work function difference between the STM tip and the BLG leads to an effective electric field acting on the BLG and results in the confining potential [Fig. 1(d)]. Then, several almost equally spaced resonances, which are attributed to the confined bound states in the BLG QD, are observed in the STS spectra [Fig. 3(b)]. In the center of the BLG QD, the LDOS of the bound states are mainly contributed by the angular momentum $M = \pm 1$. The level spacing of the confined bound states does not change very much with the tip-sample distance, as shown in Fig. 3(b),

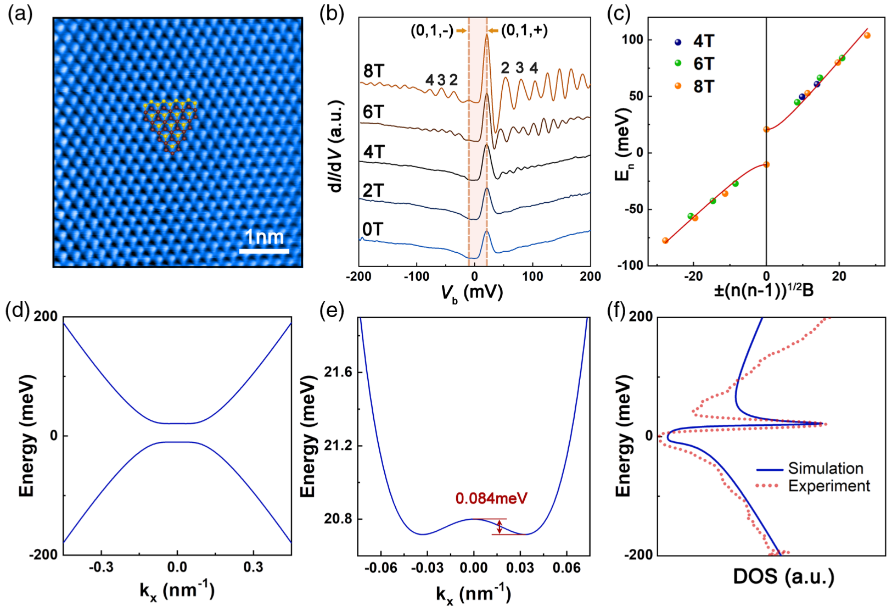

FIG. 2. (a) A 5×5 nm^2 atomic-resolved STM image ($V_{\mathrm{sample}} = 800$ mV, $I = 200$ pA) of the Bernal-stacked BLG. The triangular graphene lattices of the Bernal-stacked BLG are overlaid onto the image. (b) Landau level spectra of the BLG for various magnetic fields. Curves are shifted vertically for clarity. The Landau level peak indices are marked, and the gap is labeled by shadows. (c) The Landau level energies for different magnetic fields obtained from (b) against $\pm[n(n-1)]^{1/2}B$. (d) Calculated low-energy dispersions of the Bernal-stacked BLG. (e) An enlarged image of the calculated flat band dispersion in (d). (f) Experimental and calculated DOS of the top layer as a function of energy.

which indicates that the decrease of the tip height does not change the potential profile but increases the signal-to-noise ratio in the tunneling spectra.

To explore the Berry-phase-induced valley-polarized energy spectra in the BLG QD, we carried out STS measurements in magnetic fields with a small interval of the magnetic field $\Delta B = 0.05$ T, as shown in Fig. 4(a) (left panel). With increasing magnetic fields, a notable splitting of the bound states can be observed. At 1 T, the splitting is about 10 meV, which is about 100 times larger than that of Zeeman splitting for spin. When the magnetic field increases to about 3 T, two adjacent split states merge into a new state. By further increasing the magnetic field, the bound states condensed into Landau levels of massive Dirac fermions (see Figs. S4 and S5 in the Supplemental Material [29]), which helps us to completely remove the charging effect as the origin of the peaks in the spectra [13,51–53]. The above feature reminds us of the Berry-phase-induced valley-polarized energy spectra in the BLG QDs [19]. According to the semiclassical EBK quantization rule [19,28], one has

$$\oint_{C_r} \Pi_r dr = 2\pi\left(n + \frac{1}{2}\right) + \gamma \tag{1}$$

for the valley K and

$$\oint_{C_r} \Pi_r dr = 2\pi\left(n + \frac{1}{2}\right) - \gamma \tag{2}$$

for the valley K' with the integer n. Here the Berry phases for the valleys K and K' are opposite. The left sides of Eqs. (1) and (2) are dimensionless. Since Π_r (the radial momentum) and the Berry phase γ are functions of energy E, Eqs. (1) and (2) determine the behaviors of the valley-related bound states in the QDs (see Fig. S6 and Supplemental Material for details of the calculation [29]). When $\gamma = 0$, π, or 2π, the bound states for the valleys K and K' are degenerate. In other situations, the bound states for the valleys K and K' are split. Therefore, when γ is continuously tuned from π to 2π, the bound states will experience the unusual degenerate-splitting-degenerate process of the valley degrees of freedom, as directly observed in experiment [Fig. 4(a) (left panel)]. This is essentially different from the monolayer graphene, in which γ is 0 or π, and the bound states in the two valleys are always degenerate.

To further understand the above result, we calculated the LDOS for the BLG QD fully based on the quantum mechanics. For simplicity, we model the BLG QD by the Hamiltonian $\tilde{H}_\xi = H_\xi + U(r)$, where $U(\boldsymbol{r}) = \kappa r^2$ is the parabolic potential with the strength κ (see Supplemental Material for the rationality of the choice [29]). H_ξ is the 4×4 Hamiltonian for the ungated BLG

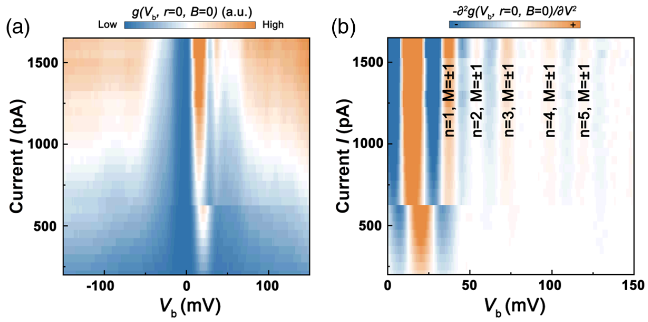

FIG. 3. (a) A color plot of the dI/dV spectra measured at different tip-sample distances Z_{tip}. The tip height decreases by increasing the tunneling current I with a fixed voltage bias. When the tip is approaching the BLG (as the tunneling current increases), the signals of the flat bands and the bound states become obvious. (b) Differential of the tunneling conductance map in (a). The feature of the bound states is more obvious. The sudden jump at about $I \approx 600$ pA may arise from the slight variation of the doping in the BLG induced by the STM tip.

$$H_\xi = v\tau_0(\xi\Pi_x\sigma_x + \Pi_y\sigma_y) + \frac{t_\perp(\tau_x\sigma_x + \tau_y\sigma_y)}{2} + \frac{\Delta_1(\tau_0+\tau_z)\sigma_0}{2} + \frac{\Delta_2(\tau_0-\tau_z)\sigma_0}{2} \tag{3}$$

in the layer $\otimes$ sublattice space, with the interlayer hopping energy $t_\perp$, the potentials Δ_1 and Δ_2 of the top and bottom layers, the valley index $\xi = \pm 1$, the Fermi velocity v, the Pauli matrices $\boldsymbol{\sigma} = (\sigma_x, \sigma_y)$ and $\boldsymbol{\tau} = (\tau_x, \tau_y)$ in the sublattice space and the layer space, and the momentum $\boldsymbol{\Pi} = (\Pi_x, \Pi_y) = (-i\hbar\partial_x - eA_x, -i\hbar\partial_y - eA_y)$ with the vector potential $\boldsymbol{A} = (A_x, A_y) = B(-y, x, 0)/2$. In the BLG QD with the rotational symmetry, the LDOS at $r = r_0$ can be expressed as $D(E) = \sum_M D_M(E)$ with $D_M(E)$ being the LDOS contributed by the angular momentum M state [19,27]. In our experiment, the on-center STM measurement mainly reflects the LDOS of the top layer of the BLG. Therefore, we present the numerical result of top-layer LDOS at the center of the BLG QD, as shown in Fig. 4(a) (right panel). The contributions from $-10 \leq M \leq 10$ are considered. To further compare the experimental data with the theoretical result, several line cuts at different magnetic fields of Fig. 4(a) are plotted in Figs. 4(b) and 4(c). The numerical calculation reproduces the main features of the experimental result, and the continuously tunable Berry phase is responsible for the degenerate-splitting-degenerate features of the LDOS. To explicitly show the effects of the Berry phase, we calculated the LDOS of the BLG QD with $r_0 = 0$ for $M = 0, \pm 1$ in Fig. S7 of the Supplemental Material [29]. The bound states of the two valleys are degenerate for the negative magnetic field with large enough absolute value due to $\gamma = 0$. When the field is increased, the bound states of the two valleys start to split because of the finite value obtained by the Berry phase. When the Berry phase is increased to π, the bound states become degenerate again, and the states of the two valleys cross each other. As the field is continuously raised, the crossing lines of the valley-related states split again because of $\gamma > \pi$. When the Berry phase achieves the value of 2π for larger enough positive magnetic fields, the two valleys become degenerate again. Finally, the states of the two valleys are recombined into degenerate Landau levels when the magnetic length is smaller than the effective radium of the QD. For other values of M, the LDOS show similar features. The switching processes of degeneracy splitting for states embodied in the LDOS are consistent with the behaviors of the continuously changed Berry phase. However, there is an obvious discrepancy between the experimental data and the theoretical result: There are two magnetic-field-independent states with a large and almost constant energy separation away from the lowest bound

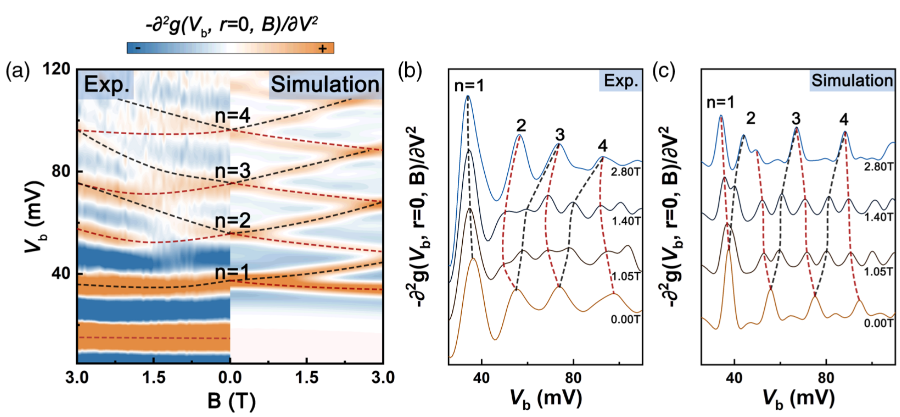

FIG. 4. (a) Experimental (left panel) and calculated (right panel) differential conductance maps versus magnetic fields B in the center of the BLG QD. Here, calculated differential conductance is proportional to the differential LDOS $-\partial^2 D(E)/\partial E^2$ of the top layer. The red (black) dashed lines guide the trend of bound states for the valley K (K'). (b),(c) Four representative line cuts in experiment and theory at different magnetic fields in (a). The red lines guide the trend of the levels for the valley K. The black lines guide the trend of the levels for the valley K'.

state [Fig. 4(a) (left panel)], which is not reproduced in theory [Fig. 4(a) (right panel)]. To explore the possible origin of the observed phenomenon, we calculated the effects of different potential profiles on the evolution of the bound states as a function of the magnetic fields, as summarized in Figs. S8 and S9 in the Supplemental Material [29]. Our calculations indicate that the profile of the potential away from the center $r = 0$ has almost no influence on the LDOS at $r = 0$, and all bound states evolve continuously through the degenerate-splitting-degenerate process when the Berry phase changes continuously from about π to 2π. The probable reason for the two magnetic-field-independent states is that they are the bound states with the same n ($n = 1$) for the valleys K and K'. The valley degenerate is lifted by the strong electron-electron interaction even in zero magnetic field, as observed in the flat bands of the MATBG [45–48,54]. As a result, these two states do not exhibit the continuous valley splitting as the magnetic field increasing from zero. Our theoretical simulation considering the electron-electron interaction really can well reproduce this unexpected phenomenon (Fig. S10 in the Supplemental Material [29]), revealing the two magnetic-field-independent states as the valley-polarized states.

In summary, large and tunable valley-polarized energy spectra are realized in the BLG QDs by continuously tuning the Berry phase. Our results demonstrate the close relationship between the valley polarization and the noninteger multiples of π of the Berry phase, which reveals the Berry phase's essential role in valleytronics. The observed large valley splitting at moderate magnetic fields sheds light on graphene-based valleytronics.

This work was supported by the National Key R&D Program of China (Grants No. 2021YFA1401900, No. 2021YFA1400100, and No. 2017YFA0303301) and the National Natural Science Foundation of China (Grants No. 12141401, No. 11974050, and No. 11921005).

Y.-N. R. and Q. C. contributed equally to this work.

[*]Corresponding author.
sunqf@pku.edu.cn
[†]Corresponding author.
helin@bnu.edu.cn

[1] D. Xiao, W. Yao, and Q. Niu, Valley-Contrasting Physics in Graphene: Magnetic Moment and Topological Transport, Phys. Rev. Lett. **99**, 236809 (2007).

[2] D. Xiao, M.-C. Chang, and Q. Niu, Berry phase effects on electronic properties, Rev. Mod. Phys. **82**, 1959 (2010).

[3] R. V. Gorbachev, J. C. W. Song, G. L. Yu, A. V. Kretinin, F. Withers, Y. Cao, A. Mishchenko, I. V. Grigorieva, K. S. Novoselov, L. S. Levitov, and A. K. Geim, Detecting topological currents in graphene superlattices, Science **346**, 448 (2014).

[4] N. M. Freitag, T. Reisch, L. A. Chizhova, P. Nemes-Incze, C. Holl, C. R. Woods, R. V. Gorbachev, Y. Cao, A. K. Geim, K. S. Novoselov, J. Burgdörfer, F. Libisch, and M. Morgenstern, Large tunable valley splitting in edge-free graphene quantum dots on boron nitride, Nat. Nanotechnol. **13**, 392 (2018).

[5] S.-Y. Li, Y. Su, Y.-N. Ren, and L. He, Valley Polarization and Inversion in Strained Graphene via Pseudo-Landau Levels, Valley Splitting of Real Landau Levels, and Confined States, Phys. Rev. Lett. **124**, 106802 (2020).

[6] Y. Shimazaki, M. Yamamoto, I. V. Borzenets, K. Watanabe, T. Taniguchi, and S. Tarucha, Generation and detection of pure valley current by electrically induced Berry curvature in bilayer grapheme, Nat. Phys. **11**, 1032 (2015).

[7] M. Sui, G. Chen, L. Ma, W.-Y. Shan, D. Tian, K. Watanabe, T. Taniguchi, X. Jin, W. Yao, D. Xiao, and Y. Zhang, Gate-tunable topological valley transport in bilayer grapheme, Nat. Phys. **11**, 1027 (2015).

[8] L. Ju, Z. Shi, N. Nair, Y. Lv, C. Jin, J. Velasco, C. Ojeda-Aristizabal, H. A. Bechtel, M. C. Martin, A. Zettl, J. Analytis, and F. Wang, Topological valley transport at bilayer graphene domain walls, Nature (London) **520**, 650 (2015).

[9] L.-J. Yin, H. Jiang, J.-B. Qiao, and L. He, Direct imaging of topological edge states at a bilayer graphene domain wall, Nat. Commun. **7**, 11760 (2016).

[10] J. Li, R.-X. Zhang, Z. Yin, J. Zhang, K. Watanabe, T. Taniguchi, C. Liu, and J. Zhu, A valley valve and electron beam splitter, Science **362**, 1149 (2018).

[11] M. Eich, F. Herman, R. Pisoni, H. Overweg, A. Kurzmann, Y. Lee, P. Rickhaus, K. Watanabe, T. Taniguchi, M. Sigrist, T. Ihn, and K. Ensslin, Spin and Valley States in Gate-Defined Bilayer Graphene Quantum Dots, Phys. Rev. X **8**, 031023 (2018).

[12] A. Kurzmann, M. Eich, H. Overweg, M. Mangold, F. Herman, P. Rickhaus, R. Pisoni, Y. Lee, R. Garreis, C. Tong, K. Watanabe, T. Taniguchi, K. Ensslin, and T. Ihn, Excited States in Bilayer Graphene Quantum Dots, Phys. Rev. Lett. **123**, 026803 (2019).

[13] Y.-W. Liu, Z. Hou, S.-Y. Li, Q.-F. Sun, and L. He, Movable Valley Switch Driven by Berry Phase in Bilayer-Graphene Resonators, Phys. Rev. Lett. **124**, 166801 (2020).

[14] L. Banszerus, A. Rothstein, T. Fabian, S. Möller, E. Icking, S. Trellenkamp, F. Lentz, D. Neumaier, K. Watanabe, T. Taniguchi, F. Libisch, C. Volk, and C. Stampfer, Electron–hole crossover in gate-controlled bilayer graphene quantum dots, Nano Lett. **20**, 7709 (2020).

[15] C. Tong, R. Garreis, A. Knothe, M. Eich, A. Sacchi, K. Watanabe, T. Taniguchi, V. Fal'ko, T. Ihn, K. Ensslin, and A. Kurzmann, Tunable valley splitting and bipolar operation in graphene quantum dots, Nano Lett. **21**, 1068 (2021).

[16] A. Knothe and V. Fal'ko, Influence of minivalleys and Berry curvature on electrostatically induced quantum wires in gapped bilayer graphene, Phys. Rev. B **98**, 155435 (2018).

[17] A. Knothe and V. Fal'ko, Quartet states in two-electron quantum dots in bilayer grapheme, Phys. Rev. B **101**, 235423 (2020).

[18] C. Gold, A. Kurzmann, K. Watanabe, T. Taniguchi, K. Ensslin, and T. Ihn, Scanning gate microscopy of localized

states in a gate-defined bilayer graphene channel, Phys. Rev. Research **2**, 043380 (2020).

[19] Z. Hou, Y.-F. Zhou, X. C. Xie, and Q.-F. Sun, Berry phase induced valley level crossing in bilayer graphene quantum dots, Phys. Rev. B **99**, 125422 (2019).

[20] K. S. Novoselov, E. McCann, S. V. Morozov, V. I. Fal'ko, M. I. Katsnelson, U. Zeitler, D. Jiang, F. Schedin, and A. K. Geim, Unconventional quantum Hall effect and Berry's phase of 2π in bilayer graphene, Nat. Phys. **2**, 177 (2006).

[21] Y. Zhang, Y. Su, and L. He, Local Berry Phase Signatures of Bilayer Graphene in Intervalley Quantum Interference, Phys. Rev. Lett. **125**, 116804 (2020).

[22] Y. Zhang, Y. Su, and L. He, Quantum interferences of pseudospin-mediated atomic-scale vortices in monolayer graphene, Nano Lett. **21**, 2526 (2021).

[23] Y.-N. Ren, M.-H. Zhang, C. Yan, Y. Zhang, and L. He, Local measurements of tunneling magneto-conductance oscillations in monolayer, Bernal-stacked bilayer, and ABC-stacked trilayer graphene, Sci. China Phys. Mech. Astron. **64**, 287011 (2021).

[24] C. Dutreix, H. González-Herrero, I. Brihuega, M. I. Katsnelson, C. Chapelier, and V. T. Renard, Measuring the Berry phase of graphene from wavefront dislocations in Friedel oscillations, Nature (London) **574**, 219 (2019).

[25] F. Ghahari, D. Walkup, C. Gutiérrez, J. F. Rodriguez-Nieva, Y. Zhao, J. Wyrick, F. D. Natterer, W. G. Cullen, K. Watanabe, T. Taniguchi, L. S. Levitov, N. B. Zhitenev, and J. A. Stroscio, An on/off Berry phase switch in circular graphene resonators, Science **356**, 845 (2017).

[26] In Ref. [13], the valley polarization and its evolution in magnetic fields of a confined bound state (the nearest one to the Fermi level) in the tip-induced BLG QD are indirectly measured by using single-electron tunneling to the bound state. The value of the valley polarization is deduced according to the energy separations of the single-electron tunneling. Therefore, the main quantum number and the energy spacing of the bound states are undetectable. This is quite different from the measurements in this work where the spectrum and its unusual degenerate-splitting-degenerate process of the valley degrees of freedom in the tip-induced BLG QD are directly measured. Then, the valley polarization of different bound states can be measured, and the values of valley splitting are directly obtained according to the energy separations between the valley-polarized states.

[27] Y. Zhao, J. Wyrick, F. D. Natterer, J. F. Rodriguez-Nieva, C. Lewandowski, K. Watanabe, T. Taniguchi, L. S. Levitov, N. B. Zhitenev, and J. A. Stroscio, Creating and probing electron whispering-gallery modes in graphene, Science **348**, 672 (2015).

[28] J. F. Rodriguez-Nieva and L. S. Levitov, Berry phase jumps and giant nonreciprocity in Dirac quantum dots, Phys. Rev. B **94**, 235406 (2016).

[29] See Supplemental Material at http://link.aps.org/supplemental/10.1103/PhysRevLett.128.206805, which includes Refs. [30–38], for sample preparation, more experimental data, details of calculation, and discussion.

[30] L.-J. Yin, L.-J. Shi, L.-Z. Yang, L.-H. Tong, and L. He, Spectroscopic characterization of Landau-level splitting and the intermediate $v = 0$ phase in bilayer graphene, Phys. Rev. B **101**, 165418 (2020).

[31] J. Lee, D. Wong, J. Velasco Jr, J. F. Rodriguez-Nieva, S. Kahn, H.-Z. Tsai, T. Taniguchi, K. Watanabe, A. Zettl, F. Wang, L. S. Levitov, and M. F. Crommie, Imaging electrostatically confined Dirac fermions in graphene quantum dots, Nat. Phys. **12**, 1032 (2016).

[32] R. G. Littlejohn and W. G. Flynn, Geometric Phases and the Bohr-Sommerfeld Quantization of Multicomponent Wave Fields, Phys. Rev. Lett. **66**, 2839 (1991).

[33] S. Keppeler, Torus Quantization for Spinning Particles, Phys. Rev. Lett. **89**, 210405 (2002).

[34] P. Carmier and D. Ullmo, Berry phase in graphene: Semiclassical perspective, Phys. Rev. B **77**, 245413 (2008).

[35] A. Kormányos, P. Rakyta, L. Oroszlány, and J. Cserti, Bound states in inhomogeneous magnetic field in graphene: Semiclassical approach, Phys. Rev. B **78**, 045430 (2008).

[36] M. A. de Gosson, *Born-Jordan Quantization: Theory and Application* (Springer, Cham, 2016).

[37] A. D. Stone, Einstein's unknown insight and the problem of quantizing chaos, Phys. Today **58**, No. 8, 37 (2005).

[38] C.-H. Park and N. Marzari, Berry phase and pseudospin winding number in bilayer graphene, Phys. Rev. B **84**, 205440 (2011).

[39] Z.-Q. Fu, Y. Zhang, J.-B. Qiao, D.-L. Ma, H. Liu, Z.-H. Guo, Y.-C. Wei, J.-Y. Hu, Q. Xiao, X.-R. Mao, and L. He, Spatial confinement, magnetic localization, and their interactions on massless Dirac fermions, Phys. Rev. B **98**, 241401(R) (2018).

[40] Y.- N. Ren, Q. Cheng, Y.-W. Liu, S.-Y. Li, C. Yan, K. Lv, M.-H. Zhang, Q.-F. Sun, and L. He, Spatial and magnetic confinement of massless Dirac fermions, Phys. Rev. B **104**, L161408 (2021).

[41] L.-J. Yin, S.-Y. Li, J.-B. Qiao, J.-C. Nie, and L. He, Landau quantization in graphene monolayer, Bernal bilayer, and Bernal trilayer on graphite surface, Phys. Rev. B **91**, 115405 (2015).

[42] L.-J. Yin, Y. Zhang, J.-B. Qiao, S.-Y. Li, and L. He, Experimental observation of surface states and Landau levels bending in bilayer graphene, Phys. Rev. B **93**, 125422 (2016).

[43] D. Marchenko, D. V. Evtushinsky, E. Golias, A. Varykhalov, T. Seyller, and O. Rader, Extremely flat band in bilayer graphene, Sci. Adv. **4**, eaau0059 (2018).

[44] L.-J. Yin, J.-B. Qiao, W.-J. Zuo, W.-T. Li, and L. He, Experimental evidence for non-Abelian gauge potentials in twisted graphene bilayers, Phys. Rev. B **92**, 081406(R) (2015).

[45] Y. Jiang, X. Lai, K. Watanabe, T. Taniguchi, K. Haule, J. Mao, and E. Y. Andrei, Charge order and broken rotational symmetry in magic-angle twisted bilayer graphene, Nature (London) **573**, 91 (2019).

[46] A. Kerelsky, L. J. McGilly, D. M. Kennes, L. Xian, M. Yankowitz, S. Chen, K. Watanabe, T. Taniguchi, J. Hone, C. Dean, A. Rubio, and A. N. Pasupathy, Maximized electron interactions at the magic angle in twisted bilayer graphene, Nature (London) **572**, 95 (2019).

[47] Y. Choi, J. Kemmer, Y. Peng, A. Thomson, H. Arora, R. Polski, Y. Zhang, H. Ren, J. Alicea, G. Refael, F. von Oppen, K. Watanabe, T. Taniguchi, and S. Nadj-Perge,

Electronic correlations in twisted bilayer graphene near the magic angle, Nat. Phys. **15**, 1174 (2019).

[48] Y. Xie, B. Lian, B. Jäck, X. Liu, C.-L. Chiu, K. Watanabe, T. Taniguchi, B. A. Bernevig, and A. Yazdani, Spectroscopic signatures of many-body correlations in magic-angle twisted bilayer grapheme, Nature (London) **572**, 101 (2019).

[49] Y.-W. Liu, Y. Su, X.-F. Zhou, L.-J. Yin, C. Yan, S.-Y. Li, W. Yan, S. Han, Z.-Q. Fu, Y. Zhang, Q. Yang, Y.-N. Ren, and L. He, Tunable Lattice Reconstruction, Triangular Network of Chiral One-Dimensional States, and Bandwidth of Flat Bands in Magic Angle Twisted Bilayer Graphene, Phys. Rev. Lett. **125**, 236102 (2020).

[50] H. Zhou, L. Holleis, Y. Saito, L. Cohen, W. Huynh, C. L. Patterson, F. Yang, T. Taniguchi, K. Watanabe, and A. F. Young, Isospin magnetism and spin-polarized superconductivity in Bernal bilayer grapheme, Science **375**, 774 (2022).

[51] G. M. Rutter, S. Jung, N. N. Klimov, D. B. Newell, N. B. Zhitenev, and J. A. Stroscio, Microscopic polarization in bilayer grapheme, Nat. Phys. **7**, 649 (2011).

[52] G. R. Holdman, Z. J. Krebs, W. A. Behn, K. J. Smith, K. Watanabe, T. Taniguchi, and V. W. Brar, Dynamic band structure and capacitance effects in scanning tunneling spectroscopy of bilayer graphene, Appl. Phys. Lett. **115**, 181601 (2019).

[53] J. Velasco Jr., J. Lee, D. Wong, S. Kahn, H.-Z. Tsai, J. Costello, T. Umeda, T. Taniguchi, K. Watanabe, A. Zettl, F. Wang, and M. F. Crommie, Visualization and control of single-electron charging in bilayer graphene quantum dots, Nano Lett. **18**, 5104 (2018).

[54] Y. Zhang, Z. Hou, Y.-X. Zhao, Z.-H. Guo, Y.-W. Liu, S.-Y. Li, Y.-N. Ren, Q.-F. Sun, and L. He, Correlation-induced valley splitting and orbital magnetism in a strain-induced zero-energy flatband in twisted bilayer graphene near the magic angle, Phys. Rev. B **102**, 081403(R) (2020).